Australian Earthquake Engineering Society 2010 Conference

Perth, Western Australia

Routine Micro-Seismic Monitoring in Mines

Aleksander J. Mendecki, Richard A. Lynch & Dmitriy A. Malovichko
Institute of Mine Seismology

November 2010

Abstract

Routine seismic monitoring in mines enables the quantification of exposure to seismicity and provides a logistical tool to guide the effort into the prevention and control of, and alerts to, potential rock mass instabilities that could result in rock bursts. One can define the following five specific objectives of monitoring the seismic response of the rock mass to mining: *rescue* of personnel, *prevention*, *seismic hazard rating*, *alerts* - including short term response to unexpected strong changes in certain parameters - and *back analysis* to improve the efficiency of both the mine layout design and the monitoring process. A quantitative description of seismic events and of seismicity are necessary, but not sufficient, in achieving the above objectives. The paper describes the basis of a modern digital seismic technology and seismological parameters used to quantify seismic sources and seismicity for seismic hazard assessment and rock mass stability analysis.

1 Objectives of Seismic Monitoring in Mines

In general, routine seismic monitoring enables the quantification of exposure to seismicity and provides a logistical tool to guide the effort into

prevention, rating of seismic hazards and alerts to potential rock mass instabilities that could result in rock bursts in underground mines (*Mendecki*, 1997b) and slope instabilities in open pit mines (*Lynch et al.*, 2005; *Lynch and Malovichko*, 2006; *Malovichko and Lynch*, 2006) One can define the following five specific objectives of monitoring the seismic response of the rock mass to mining (*Mendecki et al.*, 1999).

1. **Rescue:** To detect and locate potentially damaging seismic events, to alert management and to assist in rescue operations.

2. **Prevention**: To compare the observed and the expected seismic rock mass response to mining. To confirm the rock mass stability related assumptions made during the design process and enable an audit of, and corrections to, the particulars of a given design while mining.

3. **Seismic Hazard Rating**: To quantify the exposure to seismicity and to monitor its spatial and temporal changes. To classify the observed spatial and temporal seismic patterns into an agreed seismic hazard rating system.

4. **Alerts**: To detect strong and unexpected changes in the spatial and/or temporal behaviour of seismic parameters that could lead to instability, affecting working places immediately or in the short term.

5. **Back Analysis**: To improve both the mine design and the seismic monitoring processes. Particularly important is thorough and objective back analysis of larger rock mass instabilities even if they did not result in injuries, loss of life or damage. Back analysis should form the basis for a regular critical review of the applied seismic risk management strategy, guidelines and procedures.

A quantitative description of seismic events and seismicity is considered the minimum requirement to achieve the above objectives.

2 The Importance of Location

The location of a seismic event is assumed to be a point within the seismic source that triggered the set of seismic sites used to locate it. The complexity of processes at the source, however, may complicate the location of a seismic event. If a slow or weak rupture starts at a certain point, the closest site(s) may record waves radiated from that very point while

others may only record waves generated later in the rupture process by a higher stress drop patch of the same source. One needs to be specific in determining the arrival times of different phases if the location of rupture initiation is sought, otherwise the location will be a statistical average of different parts of the same source.

A reasonably accurate location is important for the following reasons :

- To indicate the location of potential rock bursts.
- All subsequent seismological processing, e.g. quantification of seismic sources, attenuation or velocity inversion, depends on location.
- All subsequent interpretation of individual events depends on location, e.g. events far from active mining, close to a shaft or, in general, in places not predicted by numerical modelling, may raise concerns.
- All subsequent interpretation of seismicity, e.g. clustering and specifically localization around planes, migration, spatio-temporal gradients of seismic parameters and other patterns are judged by their location and timing.

Since the source of a seismic event has a finite size, the attainable location accuracy of all seismic events in a given area should be within the typical size of an event of that magnitude which defines the sensitivity of the seismic network for that area, i.e. the minimum magnitude, m_{min}, above which the system records all events with sufficient signal to noise ratio, see Table 1.

Table 1: Recommended minimum location accuracy for different network sensitivities as defined by the m_{min}. Approximate source sizes for a given m_{min} for stress drops 0.5 MPa and 0.1 MPa, are also given as a reference.

Sensitivity, m_{min}, source size, [m]	1.0 65-110	0.5 35-64	0.0 20-35	-0.5 12-20	-1.0 6-12	-1.5 4-6	-2.0 2-4
Location Accuracy, [m]	100	75	40	20	15	10	5

Given the high quality data from at least 6 three component sites of reasonable configuration, the error may be reduced to less than 3% of the average hypocentral distance to the sites used in the location.

3 Quantification of Seismic Sources

A seismic event is considered to be described quantitatively when apart from its timing, t, and location, $X = (x, y, z)$, at least two independent parameters pertaining to the seismic source namely, seismic potency, P, which measures co-seismic inelastic deformation at the source and radiated seismic energy, E, are determined reliably.

Seismic Potency. Seismic potency P represents the volume of rock, of whatever shape, associated with co-seismic inelastic deformation at the source (*Ben-Menahem and Singh*, 1981, *King*, 1978). The scalar seismic potency [m^3], is the product of the strain change and the source volume

$$P = \Delta\epsilon V. \tag{1}$$

For a planar shear source, the potency is defined as $P = \bar{u}A$, where A is the source area and $\bar{u}$ is the average slip. P is expressed in [m·m^2].

At the source, seismic potency is the integral of the source time function over the duration. At the recording site potency is proportional to the integral of the P or S-wave displacement pulse corrected for the far-field radiation pattern $u_{corr}(t)$

$$P_{P,S} = 4\pi v_{P,S} R \int_0^{t_s} u_{corr}(t)dt, \tag{2}$$

where $v_{P,S}$ is P or S-wave velocity, R distance from the source, t_s is source duration and $u(0)$ = 0 and $u(t_s)$ = 0. It is most frequently estimated in frequency domain from the amplitude of the low frequency displacement spectra Ω_0 of the recorded waveforms (*Keilis-Borok*, 1959)

$$P_{P,S} = 4\pi v_{P,S} R \frac{\Omega_{0,P,S}}{\Lambda_{P,S}} \tag{3}$$

where $\Lambda_{P,S}$ is the root-mean-square value for the radiation pattern of far-field amplitudes averaged over the focal sphere and Λ_P = 0.516 for P-wave and Λ_S = 0.632 for S-wave (*Aki and Richards*, 2002).

Seismic Energy. The energy release during fracture and frictional sliding is due to the transformation of elastic strain into inelastic strain. This transformation may occur at different rates ranging from slow creep-like events to very fast dynamic seismic events with an average velocity of deformation at the source of up to a few meters per second. Slow type events have a long time duration at the source and thus radiate predominantly lower frequency waves, as opposed to dynamic sources of the same size.

Since excitation of seismic energy can be represented in terms of temporal derivatives of the source function one may infer that a slower source process implies less seismic radiation. In terms of fracture mechanics, the slower the rupture velocity, the less energy is radiated; the quasi-static rupture would radiate practically no energy.

In time domain the radiated seismic energy of the P or S-wave is proportional to the integral of the radiation pattern corrected far-field velocity pulse squared $\dot{u}^2(t)$ of duration t_s,

$$E_{P,S} = \frac{8}{5}\pi\rho v_{P,S} R^2 \int_0^{t_s} \dot{u}^2_{corr}(t)dt, \tag{4}$$

where ρ is rock density, $v_{S,P}$ is S or P-wave velocity and R is the distance from the source. In the far field of seismic observations the P and S-wave contribution to the total radiated energy are proportional to the integral of the square of the P and S velocity spectrum. For a reasonable signal to noise ratio in the bandwidth of frequencies available on both sides of the dominant (corner) frequency f_0, the determination of that integral from waveforms recorded by seismic network is fairly objective. The high frequency component of seismic radiation needs to be recorded by the seismic system if a meaningful insight into the stress regime at the source is to be gain.

Apparent Stress. The apparent stress σ_A is defined as the ratio of the radiated seismic energy E to potency P

$$\sigma_A = \frac{E}{P} \tag{5}$$

and it measures the amount of radiated seismic energy per unit volume of inelastic deformation at source (*Aki*, 1966; *Wyss and Brune*, 1968).

Energy Index. The notion of comparing the radiated energies of seismic events of similar potency can conveniently be translated into a practical tool called the energy index, EI (*van Aswegen and Butler*, 1993). The energy index of an event is the ratio of the observed radiated seismic energy of that event E, to the average energy $\bar{E}(P)$ radiated by events of the observed potency P taken from $\log \bar{E} = d \log P + c$, for the area of interest - Figure 1

$$EI = \frac{E}{\bar{E}(P)} = \frac{E}{10^{d \log P + c}} = 10^{-c} \frac{E}{P^d}\,, \tag{6}$$

which for d=1.0 would be proportional to the apparent stress. The higher the energy index the higher the driving stress at the source of the event at the time of its occurrence.

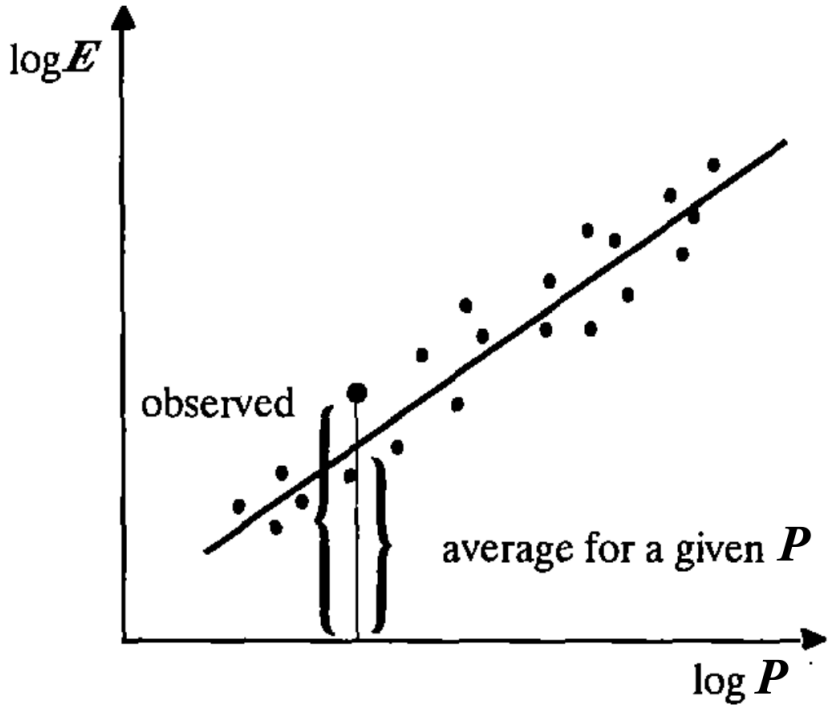

Figure 1: Energy index concept, *after Mendecki* (1997a)

Apparent Volume. Source volume can be estimated from, $V = P/\Delta\epsilon$, and it measures the volume of rock with the inelastic shear strain change $\Delta\epsilon$. While potency can be reliably derived from waveforms, the strain change, $\Delta\epsilon = c \cdot P f_0^3$, is model dependent and it suffers from its cubic dependency on corner frequency f_0. Therefore a relatively small uncertainty in f_o can cause a large uncertainty $\Delta\epsilon$ and, consequently, in the source volume V. More stable parameter then is the apparent volume (*Mendecki*, 1993) that replaces the strain drop with apparent strain:

$$V_A = \frac{P}{\epsilon_A} = \frac{\mu P^2}{E}. \tag{7}$$

where μ is the rigidity of the rock. Apparent volume, like apparent stress, depends on seismic potency and radiated energy, and, because of its scalar nature, can easily be manipulated in the form of cumulative or contour plots.

Stress and Strain Change. A seismic system can measure only that portion of strains, stresses or rheology of the process which is associated with recorded seismic waves. The wider the frequency and amplitude range and the higher the throughput of the system, the more reliable and more relevant the measured values of these parameters become.

Seismic waveforms provide information about the strain and stress changes at the source. The source of a seismic event associated with a weaker geological feature or with a softer patch in the rock mass yields more slowly under lower differentiial stress, and radiates less seismic energy per unit of inelastic co-seismic deformation, than an equivalent source within strong and highly stressed rock. By comparing radiated seismic energies of seismic events with similar potencies one can gain insight into the stresses acting within the part of the rock mass affected by these events - see Figure 2.

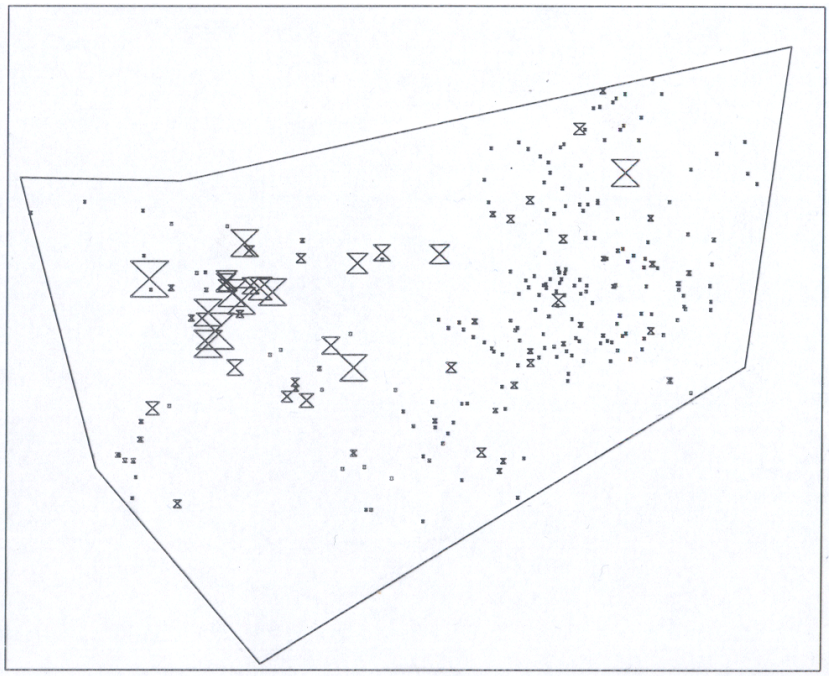

Figure 2: Apparent stresses of selected seismic events with equal local magnitudes m = 1.0 in a South African Gold Mine. The ratio of the highest to the lowest apparent stress on this figure is nearly 100.

The routine estimates of seismic potency and radiated seismic energy from waveforms are relatively inaccurate, with uncertainties, as measured from the scatter of processed data around the model, from 50% for well behaved waveforms to over 100% for complex ones. However, the variation in radiated seismic energy of seismic events with similar potency occurring in different stress and/or strain regimes at the same mine is considerably greater than the uncertainty in measurements and the error propagation in processing. Thus, while these uncertainties influence the resolution obtainable negatively, they should not prevent the quantitative interpretation

and comparison of seismic strain and stress changes between different time intervals and/or between different areas covered by the same seismic system.

Having recorded and processed a number of seismic events within a given volume of interest ΔV over time Δt, one can then quantify the changes in the strain and stress regimes and in the rheological properties of the rock mass deformation associated with the seismic radiation.

This presents an opportunity to validate the results of numerical modelling of the design process. In the numerical modelling practice the assumption of the same elastic constants within a given volume of rock, $\sigma =$ constant $\cdot \epsilon$, makes strain and stress distribution equivalent. However, seismically inferred stress and strain changes are independent. Seismic strain associated with seismic events in a given volume is proportional to seismic potencies, $\epsilon_s \sim \sum P$, and seismic stress is proportional to the ratio of seismic energies to seismic potencies, $\sigma_s \sim \sum E / \sum P$. Since seismic potency and the radiated energy are independent, the contours of seismic strain and seismic stress may be qualitatively different, reflecting differences in stress regime and/or rock mass properties - see Figure 3 as an example. It is the difference between the modelled stress and/or strain distributions and the observed ones that need to be explained and reconciled with the design while mining (*Mendecki et al.*, 1999).

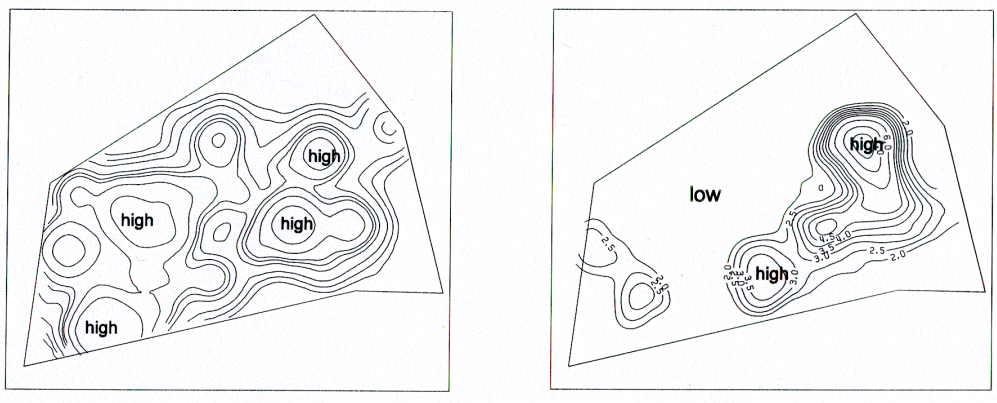

Figure 3: Contours of seismic strain (left) and seismic stress (right) for seismic events of all magnitudes in the area shown in Figure 1. Please note the qualitative difference between the distributions of seismic strains and stresses.

4 Seismic Source Mechanism

4.1 Representation of seismic sources

The low frequency component of seismic waves generated by the majority of dynamical processes in rock masses can be described using a set of force dipoles acting at some point within the elastic source (*Backus and Mulcahy*, 1976). The exceptions are processes accompanied by movement of mass in the source - this seismic radiation is characterized by a single force (*Takei and Kumazawa*, 1994). Thus a set of 9 basic force dipoles, comprising the seismic moment tensor M_{ij}, is a universal descriptor of seismic radiation for a wide range of source processes including mining-induced seismicity. For instance, a planar shear failure may be described by two dipoles with opposite moments, while radiation of a symmetric explosive source may be described by three orthogonal linear dipoles. Another fundamental description of seismic radiation – the potency tensor P_{ij}- has become widespread of late. This quantity characterises the virtual elastic unconfined deformation of the source material which has the same seismic effect as the actual inelastic deformation. The benefits of P_{ij} over M_{ij} is the fact that the potency tensor doesn't depend on (essentially unknown) parameters of material in the vicinity of the source.

Thereby tensors M_{ij} and P_{ij} represent elegant structures providing two-way connection between source processes and their seismic signals. On the one hand a set of equivalent force dipoles M_{ij} (or equivalent elastic deformations measures P_{ij}) could be specified for practically all processes, and seismograms could be synthesized for these equivalent dipoles or deformations. On the other hand inversion of seismic moment tensor or potency tensor can be performed for recorded seismic waveforms, with the subsequent benefits of our understanding of the source mechanisms.

4.2 Interpretation of the mechanisms

The initial step of interpretation usually consists of decomposition of tensor M_{ij} or P_{ij} into two parts. Seismic moment and potency tensors possess property of symmetry of components for the majority of source processes (the exceptions can be found again in *Takei and Kumazawa*, 1994) and as a result they will have only two parts – the isotropic and deviatoric components. The isotropic component characterizes change in volume of material in the seismic event source. For instance, in the case of a planar shear

fault this component will be zero. The deviatoric component describes the inelastic change of shape of material in the source.

A more specific interpretation of the obtained seismic moment or potency tensor is possible if some specific source model is assumed. For example, two alternative variants of geometrical parameters of faulting (orientation of the plane and direction of the faulting) can be estimated according to the deviatoric components of M_{ij} or P_{ij} if planar shear faulting is assumed to be the source process.

4.3 Visualization and estimation of the mechanisms

The common visualization of seismic source mechanisms is a representation of P-waves polarities in far-field zone (compressions or dilatations) on a virtual sphere centered with source (the focal sphere). This sphere with associated polarities is usually represented in a form of horizontal projection. In the case of shear faulting the focal sphere is divided by two nodal planes onto 4 quadrants having alternate polarities (Figure 4a). The regions of compression and dilatation phases will have another configuration for different types of sources. For example, in the case of complex failure including simultaneous rupture of shear and tensile cracks the mechanism will contain isotropic (explosive) component giving rise to larger area of positive polarities of P-waves in comparison with the area of negative ones (Figure 4b).

Currently there is a wide spectrum of techniques for the estimation of seismic source mechanisms for mine seismicity. Some techniques operate within the bound of specific model of the source – generally this model is a planar shear faulting (*Voinov and Selivonik*, 1998; *Younga and Fedotova*, 2000). Others give the possibility to obtain universal characteristics in the form of tensors M_{ij} or P_{ij} (*Mendecki*, 1993; *Trifu et al.*, 2000). Also the techniques are discriminated according to type of input data – some of them are based only on polarities and amplitudes of P- and S-waves while others involve full waveforms.

Some features of mine induced seismicity have aided the estimation of seismic source mechanisms. Firstly the seismic arrays installed in mines are usually 3-dimensional, much better than the 2-dimensional arrays used in crustal and regional seismic monitoring. Secondly the medium may usually be assumed to be homogeneous and isotropic, unlike the large differences present over hundreds or thousands of kilometers in the Earth's crust.

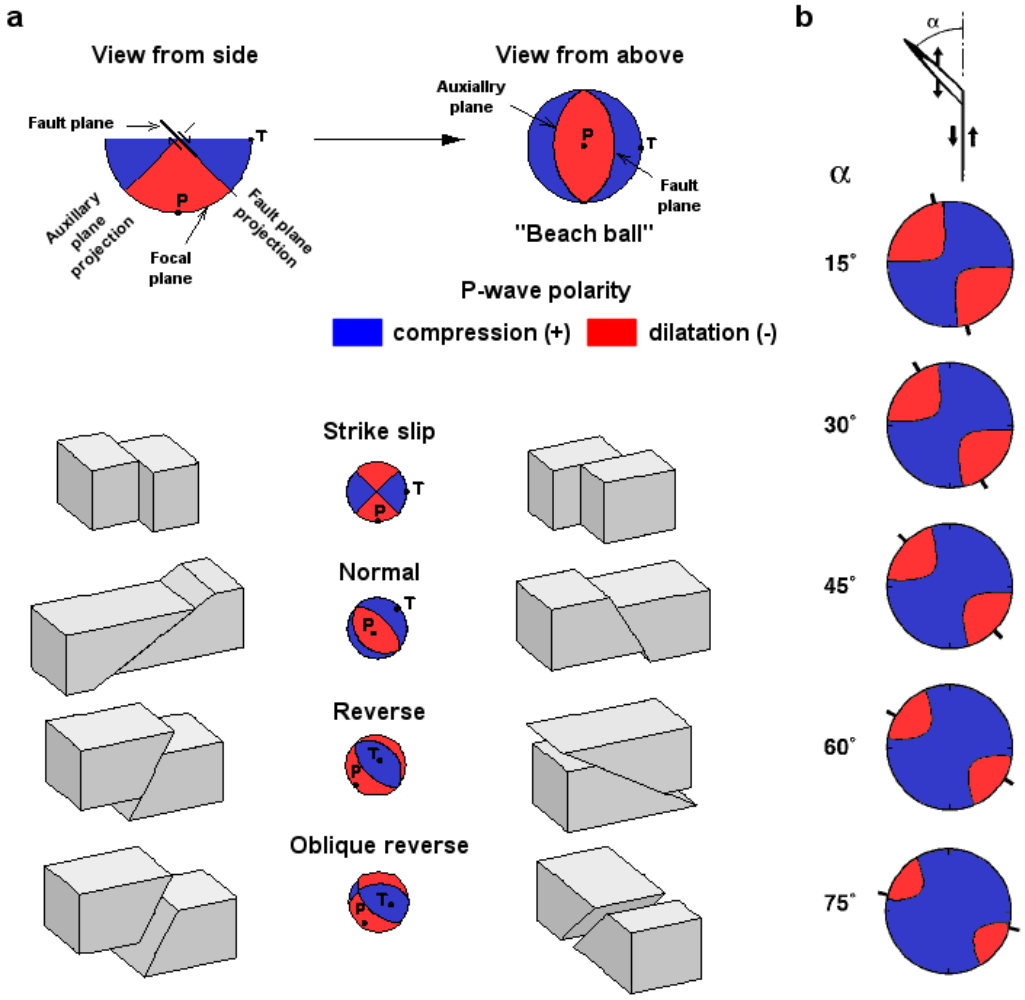

Figure 4: Visualization of mechanisms of seismic events: the distribution of first motion polarities on the focal sphere for different source mechanisms is shown in (a) (from *USGS*, 1996), while in (b) the source mechanism representation for the case of combined shear and tensile fractures are shown (from *Julian et al.*, 1998).

An example of seismic source mechanism invertion for mines is presented in Figure 5. The mechanisms of 7 large events which took place during a 6 year period and their 32 aftershocks in a section of a block-caving mine are shown as “beach balls”. The cave surface is shown in yellow.

Attention should be paid to two aspects in this example:

- The insignificance of isotropic components in mechanisms of both

main shocks and aftershocks (the “beach-balls” shown in Figure 5 are similar to ones presented in Figure 4a). This implies that shear failure dominates the source mechanism.

- The uniformity of the mechanisms. Evidently that the centers of positive P-waves polarity regions have vertical orientation. The centers of the negative polarities regions have North-South orientation. Such uniformity indicates the consistency of factors that initiated these large events during the long period of time (six years!).

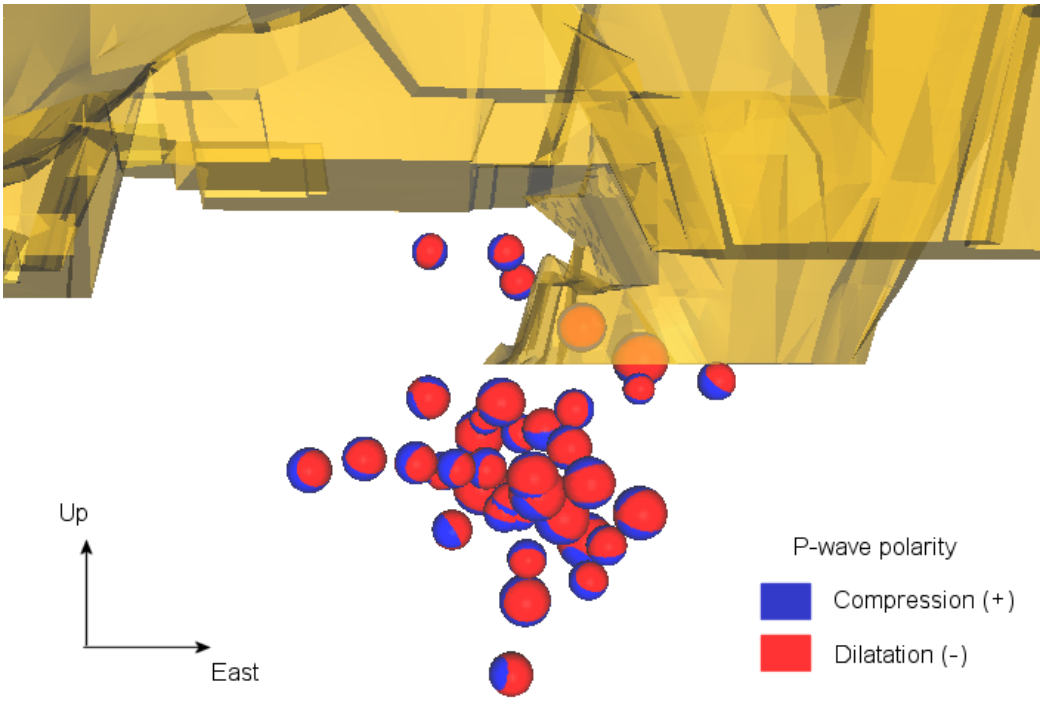

Figure 5: Mechanisms of 7 large seismic events and their 32 aftershocks in a large block-cave mine, recorded during a 6-year period.

4.4 Application of information about seismic source mechanism in mines

The source mechanism and their simplified analysis as demonstrated above yields new knowledge about seismicity which is complementary to information presented in Chapter 3. In general the estimation of seismic source mechanisms for mine seismicity allows some important practical issues to be investigated:

- Investigation of the causes of a specific rockburst. In this case the parameters of the mechanism of seismic event associated with the rockburst (orientation of possible nodal planes and slip vectors) are compared with characteristics of known geological features in the vicinity of the source.

- Estimation of stress state of rock mass. A collection of geometrical parameters of the sources of seismic events that occurred in some rock volume contains information about stress state of this volume, i.e. about direction of principal axes of stress and ratio of their amplitudes (*Dubinski and Stec*, 2001).

5 Quantification of Seismicity (*Mendecki*, 1997a)

The few most frequent quantities derived from waveforms are: time t, location $X = (x, y, z)$, potency P including its tensor P_{ij} and radiated energy E. If seismicity is considered as a group of seismic events confined to a given volume ΔV and time Δt then, in addition to statistical moments, one can define a number of parameters based on the following quantities:

- average time between consecutive events $\bar{t}$,

- average distance between consecutive events $\bar{X}$, including source sizes,

- sum of seismic potencies $\sum P$ or $\sum P_{ij}$, or moments

- sum of radiated energies $\sum E$.

The following parameters describe the statistical properties of co-seismic deformation and associated changes in the strain rate, stress and the rheology of the process. The usefulness of these parameters depends on the definition of the group of events. It is important that the selection of ΔV and Δt be guided by the characteristic space and time scales associated with the processes under study.

5.1 Seismic Strain, Stress and Stiffness

The average seismic strain tensor ϵ_{ij}, produced by a number of events that have occurred within the volume ΔV over the period of time $\Delta t = t_2 - t_1$ is proportional to the sum of their potency tensors (*Brune*, 1968; *Kostrov*, 1974; *Kostrov and Das*, 1988)

$$\epsilon_{s_{ij}}(\Delta V, \Delta t) = \frac{1}{2\Delta V} \sum_{t_1}^{t_2} P_{ij}. \tag{8}$$

The average seismic strain rate tensor then is

$$\dot{\epsilon}_{s_{ij}}(\Delta V, \Delta t) = \frac{1}{2\Delta V \Delta t} \sum_{t_1}^{t_2} P_{ij} \tag{9}$$

The average seismic stress tensor, $\sigma_{s_{ij}}$, has been defined by *Kostrov*, 1974; *Kostrov and Das* (1988) as

$$\sigma_{s_{ij}}(\Delta V \Delta t) = \frac{1}{\dot{\epsilon}_{s_{ij}} \Delta V \Delta t} \sum_{t_1}^{t_2} E = \frac{2 \sum_{t_1}^{t_2} E}{\sum_{t_1}^{t_2} P_{ij}}. \tag{10}$$

As tensors, seismic strain, strain rate and seismic stress have the same principal axes. The ratio of seismic stress to seismic strain can then be taken as the seismic stiffness modulus K_s,

$$K_s(\Delta V, \Delta t) = \frac{\sigma_{s_{ij}}}{\epsilon_{s_{ij}}} = \frac{4\Delta V \sum_{t_1}^{t_2} E}{\left(\sum_{t_1}^{t_2} P_{ij}\right)^2}. \tag{11}$$

Seismic stiffness is a scalar and measures the rock mass ability to resist seismic deformation with increasing stress.

5.2 Seismic Viscosity and Relaxation Time

The rock mass resistance to seismic deformation can also be measured by seismic viscosity, η_s, defined as the ratio of seismic stress to seismic strain rate (*Kostrov and Das* (1988))

$$\eta_s(\Delta V, \Delta t) = \frac{\sigma_{s_{ij}}}{\dot{\epsilon}_{s_{ij}}} = \frac{4\Delta V \Delta t \sum_{t_1}^{t_2} E}{\left(\sum_{t_1}^{t_2} P_{ij}\right)^2} \quad \nu_s = \frac{\eta_s}{\rho}\,, \tag{12}$$

where ν_s is the kinematic viscosity and ρ is density. Elastic properties govern processes with a characteristic time scale less than the relaxation time $\tau = \eta/\mu$, [s], where η is viscosity and μ rigidity.

$$\tau_s(\Delta V, \Delta t) = \frac{\eta_s}{\mu} = \frac{4\Delta V \Delta t \sum_{t_1}^{t_2} E}{\mu \left(\sum_{t_1}^{t_2} P_{ij}\right)^2} \tag{13}$$

5.3 Seismic Diffusivity and Schmidt Number

The statistical difusivity can be defined as

$$d_s(\Delta V, \Delta t) = \frac{\left(\bar{X}\right)^2}{\bar{t}} \tag{14}$$

where $\bar{X}$ is the mean distance between consecutive events and $\bar{t}$ is the mean time between events. Seismic Schmidt number, that measures the complexity of seismic deformation, is defined by

$$Sc_s(\Delta V, \Delta t) = \frac{\nu_s}{d_s} = \frac{4\Delta V \Delta t \left(\bar{t}\right) \sum_{t_1}^{t_2} E}{\rho \left(\bar{X}\right)^2 \left(\sum_{t_1}^{t_2} P_{ij}\right)^2} \tag{15}$$

Note that the Schmidt number contains all four basic parameters that describe seismicity, namely: $\bar{t}$, $\bar{X}$, $\sum P$ and $\sum E$.

5.4 Seismicity and Stability

In general the stability of the rock mass subjected to mining can be related to its stiffness, i.e. its ability to resist deformation with increasing stress. While the overall stiffness of the rock mass is being maintained the seismic potency production, $\sum P$, is expected to be proportional to the volume mined, $\sum P \sim V_m$.

As mining progresses the overall stiffness of the rock mass is being degraded and the rate of potency production per unit of V_m may increase. With further degradation in stiffness, the response may become nonlinear with accelerating potency release, $\sum P \sim (\sum V_{meff})^{\gamma}$, associated with an increase in activity rate, $1/\bar{t}$, signifying potential for larger instabilities.

The dynamics of such instability expressed by the apparent stress, $\sigma_A = E/P$, depends on the ratio of the stiffness of the potentially unstable volume of rock to the stiffness of the surrounding rock mass. The higher this ratio the more energy will be released per unit of inelastic deformation at the source.

Given these observations, searches for signs of the stress softening phase that precedes seismic instability reduces to analysis of the time histories of energy index and cumulative apparent volume, as proxies for seismic stress and strain, respectively. A period of increasing energy index with a normal rate of cumulative apparent volume (the stress hardening phase) followed by a period of dropping energy index and simultaneously accelerating cumulative apparent volume (the stress softening phase) constitutes an indication of potential future instability. With high resolution micro-seismic arrays, such patterns have been detected before many large seismic events - see Figures 6 and 7.

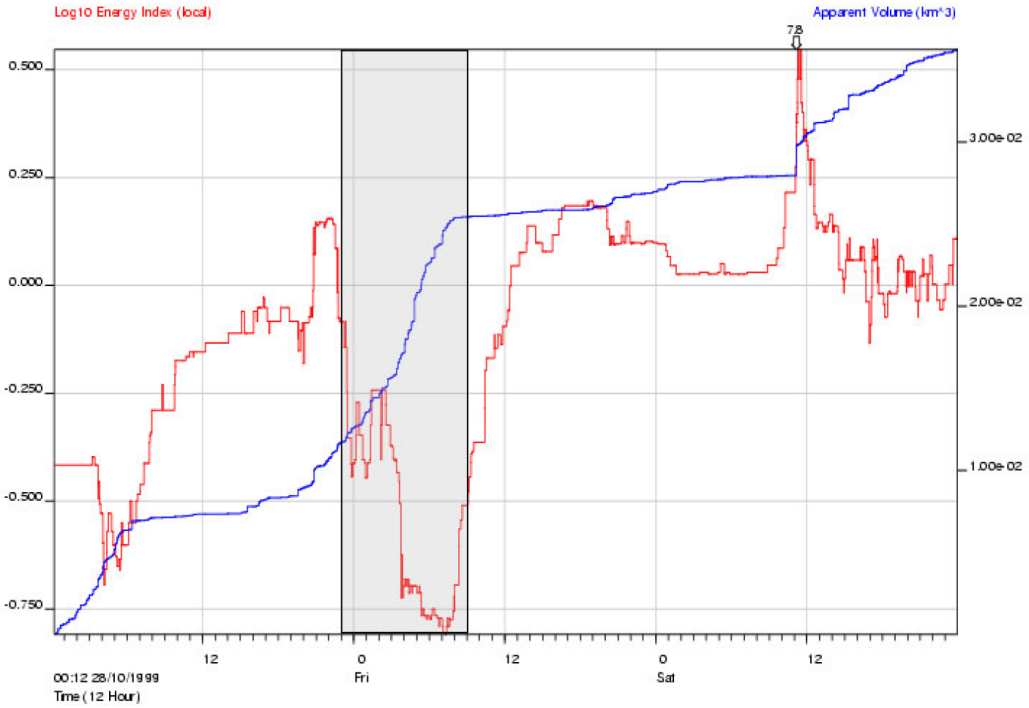

Figure 6: The characteristic pattern of dropping energy index and accelerating cumulative apparent volume 30 hours prior to a large seismic event (local magnitude 2.4 in this case), from seismic data recorded at TauTona gold mine in South Africa. Data from the period of stress softening (shaded zone) can be used to spatially identify the zone of the future instability to within about 100 m - from *Lynch and Mendecki* (2001).

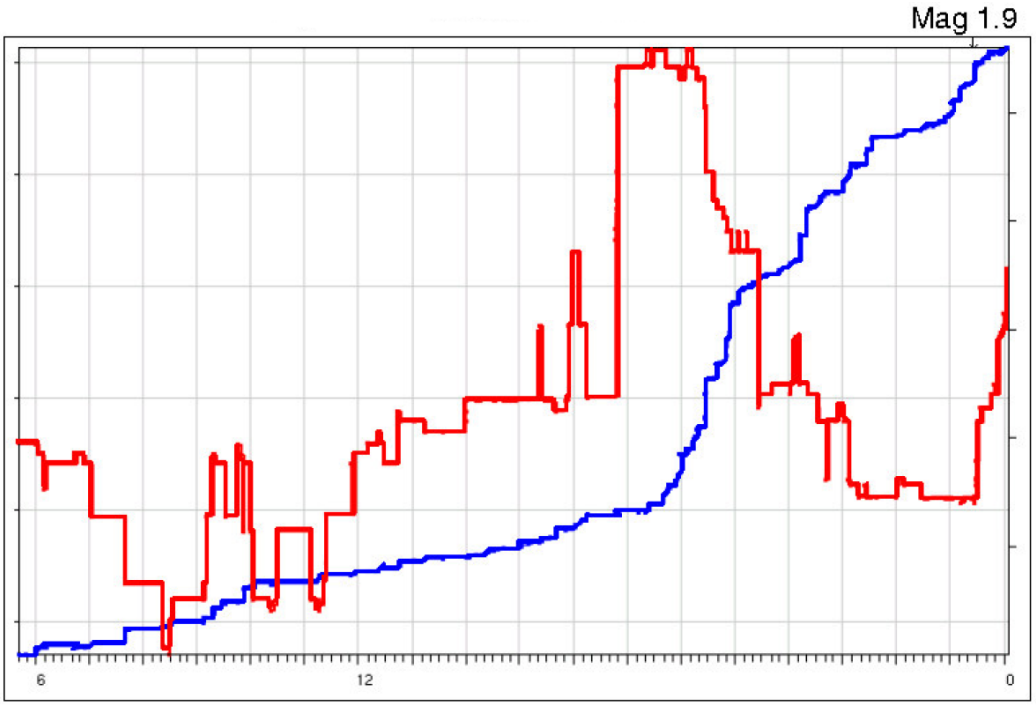

Figure 7: The characteristic pattern of dropping energy index and accelerating cumulative apparent volume prior to a large seismic event (local magnitude 1.9 in this case), from seismic data recorded at TauTona gold mine in South Africa. This time the stress softening phase is detected 6 hours prior to the large event and continues unabated until the instability - from *Lynch and Mendecki* (2004).

Another guiding idea in the interpretation of seismic activity is the concept of self-organization into critical state, i.e. a state at which the correlation length becomes comparable with the system size and at which the system can develop and maintain reproducible relationships among its distant parts. One would expect an increase in the mean distance between consecutive events, $\bar{X}$. It is assumed that the growth of long-range correlations within the rock mass allow for progressively larger events to be generated. Intermittently, correlations may reach or even exceed the size of the observed area, creating conditions conducive for large instabilities. At this stage the system's sensitivity to external or internal disturbances would diverge offering predictability. The following equations depict the expected qualitative changes in seismic parameters associated with unstable rock mass behaviour.

$$\frac{\text{energy index}}{\text{apparent volume}} = \frac{\searrow}{\nearrow} = \Downarrow \tag{16}$$

$$\textbf{viscosity}: \quad \eta_s = \frac{\textbf{stress}}{\textbf{strain rate}} = \frac{\searrow}{\nearrow} = \Downarrow \tag{17}$$

$$\textbf{diffusivity}: \quad d_s = \frac{(\textbf{distance between events})^2}{\textbf{time between events}} = \frac{\nearrow}{\searrow} = \Uparrow \tag{18}$$

The Figure 8 depicts an example of the Schmidt number and apparent volume few hours after the production blasts that resulted in seismic event of magnitude m = 1.9.

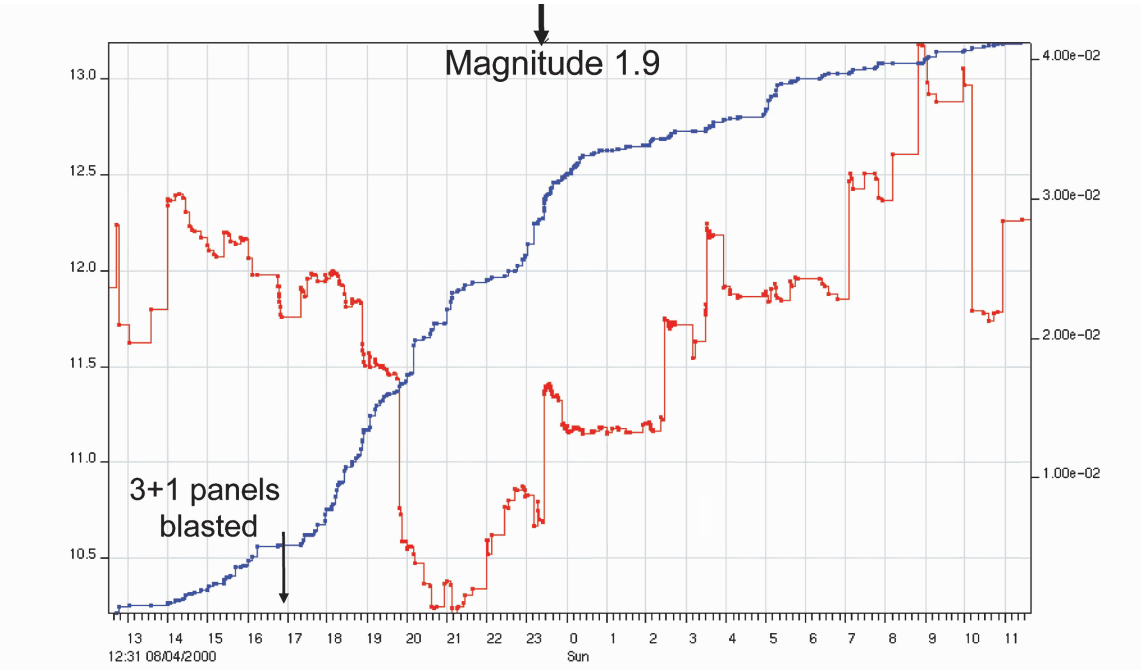

Figure 8: Schmidt number and the cumulative apparent volume over the 24 hours period showing the rock mass response to production blasts at 16h55. The large seismic event m = 1.9 occurred a few hours after the blasts and was preceeded by drop in Sc_s and accelerating V_A (*Mendecki*, 2001).

6 Seismic Monitoring Technology

To achieve meaningful results from analysis of seismic events, the seismogram data itself needs to be accurately recorded. For routine mine seismic monitoring, typical requirements are for seismic events in the moment-magnitude[1] range $-2.0 \leq m_{HK} \leq +3.5$ to be consistently recorded. Using the relation derived by *Gutenberg and Richter* (1956): $\log E = \frac{3}{2}m + 4.8$, Table 2 has been computed for reference.

Table 2: Equivalent values of potency, moment-magnitude and radiated seismic energy using the relations of *Hanks and Kanamori* (1979) and *Gutenberg and Richter* (1956) and assuming a ridigity $\mu = 30$ GPa.

Potency [m^3]	moment-magnitude	Energy [J]
0.000041	-2.0	6.3×10^1
0.00023	-1.5	3.6×10^2
0.0013	-1.0	2.0×10^3
0.0073	-0.5	1.1×10^4
0.041	0.0	6.3×10^4
0.23	0.5	3.6×10^5
1.3	1.0	2.0×10^6
7.3	1.5	1.1×10^7
41	2.0	6.3×10^7
230	2.5	3.6×10^8
1300	3.0	2.0×10^9
7300	3.5	1.1×10^{10}

To see what **frequency bandwidth** would be appropriate to monitor such typical seismic events, relations from *Keilis-Borok* (1959) and *Brune* (1971) can be combined (*Mountfort and Mendecki*, 1997) to obtain an expression for corner frequency, f_0, in terms of potency P, stress drop $\Delta\sigma$, rigidity μ and S-wave velocity v_S:

$$f_0 = \frac{2.34 v_S}{2\pi} \sqrt[3]{\frac{16\Delta\sigma}{7\mu P}} \tag{19}$$

This relation is presented graphically in Figure 9 using values of S-wave velocity commonly encountered in underground and open pit mines.

[1] The moment magnitude or Hanks-Kanamori magnitude scales with seismic potency, P, and rigidity, μ, as: $m_{HK} = \frac{2}{3}\log P + \frac{2}{3}\log\mu - 6.06$ (*Kanamori and Anderson*, 1975; *Kanamori*, 1977; *Hanks and Kanamori*, 1979)

If a typical stress drop of 1 MPa is used, it can be seen that magnitude -2.0 will produce a corner frequency of approximately 1200 Hz, while a magnitude +3.5 will produce a corner frequency of approximately 2 Hz. To accurately estimate potency from the spectral plateau, the seismogram must be recorded with a frequency content with lower limit at most $f_0/2$. To accurately estimate radiated seismic energy, the seismogram must be recorded with a frequency content with upper limit at least $5f_0$. Thus the frequency band of the seismic monitoring system (sensors and data acquisition electronics) should be at least 1 Hz to 2400 Hz for common mine situations.

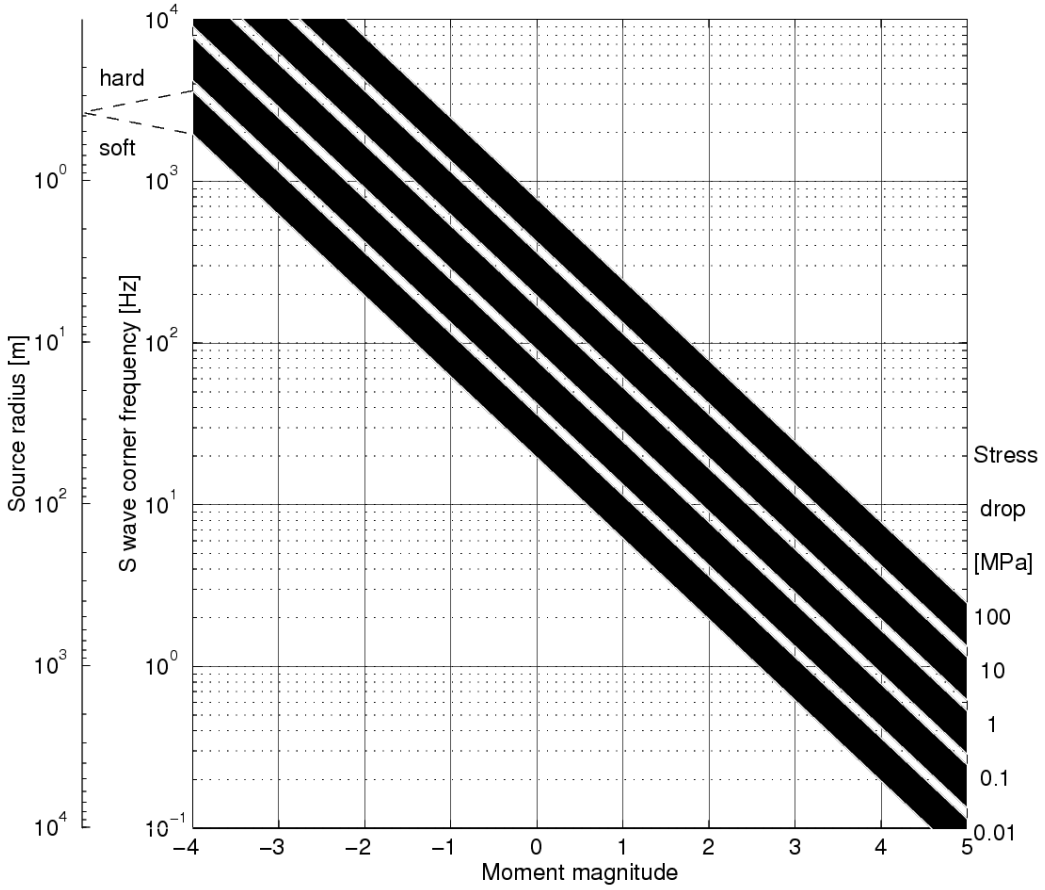

Figure 9: The relation between S-wave corner frequency and moment magnitude for a range of stress drops (producing the different series of lines) and S-wave velocities (producing the thickness of the lines) as commonly encountered in mines (*Mountfort and Mendecki*, 1997).

To estimate what **dynamic range** is required to record the typical am-

plitudes of seismic waves, an expression of *McGarr* (1991) can be used with equation 19 to produce:

$$Rv_{max} = \frac{0.0686}{\rho v_S} \sqrt[3]{\Delta\sigma^2 \mu P} \tag{20}$$

Again using a stress drop of 1 MPa, and typical values of rock density, S-wave velocity and rigidity, we can see that a magnitude +3.5 event will produce a peak seismic wave velocity of about 0.1 m/s at a seismic sensor 50 m away. A small event of magnitude -2.0 is estimated to produce a peak seismic wave velocity of about 10^{-5} m/s at a sensor 500 m from the source. In practice, this value is observed to be a little lower, at about 10^{-6} m/s. Since a signal-to-noise ratio of at least 10 is required for accurate processing of the seismogram data, the seismic system should be able to reliably record seismic signals of maximum amplitude at least 0.1 m/s, with a peak noise level of at most 10^{-7}m/s. This implies a dynamic range of the data acquisition electronics of at least 6 orders of magnitude, which is 120 dB.

Some typical seismograms from micro-seismicity recorded in mines by the ISS system are shown in Figures 10 and 11. The large range of amplitudes that must be recorded for these seismic events is evident: the small magnitude -2.0 event generates peak ground motions of about 10^{-6} m/s at 170 m from the source, while the magnitude +1.8 event generates 10^{-2} m/s at approximately the same sensor-source distance.

For small events, the seismic signals are both high frequency and low in amplitude. Surface mounted sensors tend to be noisy, are shielded from high frequencies by the fracture zone surrounding underground excavations and suffer from the variable surface amplification effect. Consequently borehole seismic sensors are preferred. The sensors are usually grouted into holes at least 7 m in depth and of diameter at least 76 mm. Figure 12 shows an IMS tri-axial 4.5 Hz borehole geophone. Such geophones have a linear response from 4 Hz to at least 2500 Hz. Passive electronics are fitted to the sensor after installation to provide a frequency-dependent amplification. This results in an effective lower frequency response of about 3 Hz, and does not introduce any noise or distortion of the signals at higher frequencies.

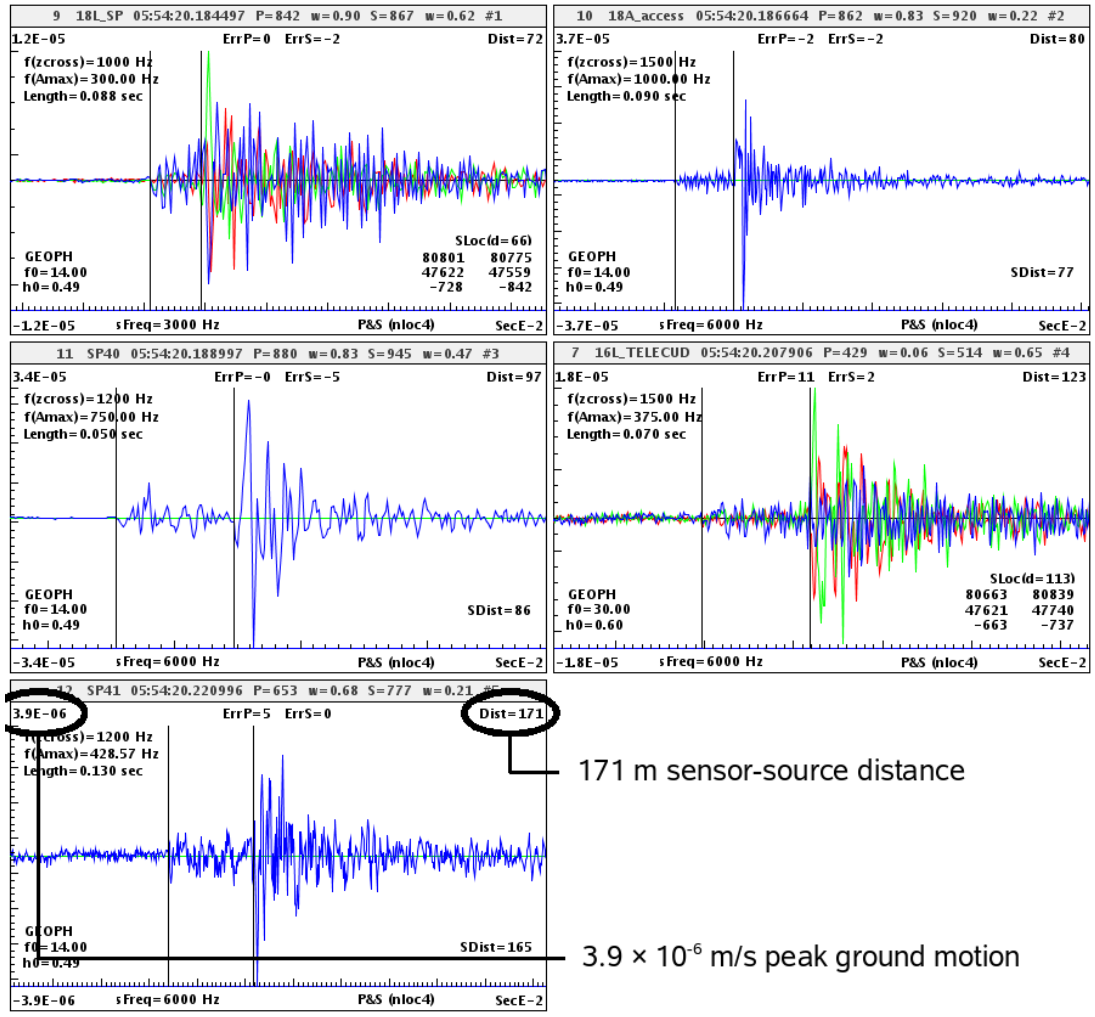

Figure 10: Seismograms recorded by an array of 14 Hz and 30 Hz borehole geophones for a magnitude -2.0 event.

Figure 11: Seismograms recorded by an array of 14 Hz and 30 Hz borehole geophones for a magnitude +1.8 event.

Figure 12: An IMS tri-axial 4.5 Hz borehole geophone. The sensor is usually installed in 10 m holes of diameter at least 76 mm. The signals from such sensors are less noisy and have less distortion than signals from surface-mounted seismic sensors.

The analogue seismic signals from geophones or accelerometers require digitisation before the data may be collected and processed on a computer. In early seismic systems the digitisation was done at a central point, and the seismic signals were carried from the sensors to this point in analogue form over copper cables. Unfortunately electrical noise prevents a large ratio between the strongest signals and the noise level, and so either small signals get obliterated by the induced electrical noise, or else a pre-amplifier is used in which case the strongest signals become clipped. Thus these 'analogue' seismic systems do not have sufficient dynamic range to meet the criterion dicussed previously in this section. For this reason, the ISS system uses distributed seismic stations near each of the sensors to digitise the signals. Then digital signals are transmitted from the stations to the central point, and so the problem of induced electrical noise is avoided.

To minimise the requirements of the digital data transmission rate, only seismograms that have been recorded consistently by a number of seismic stations are transmitted to the central site. In this way, the sampling rate at the seismic stations can be much higher than the digital communications rate to the central site.

The latest GS technology (see Figure 13) is capable of sampling rates up to 48000 Hz and uses a 32-bit over-sampled analogue-to-digital converter to achieve a dynamic range of 129 dB at 6000 Hz sampling. A digital sigma-delta anti-aliasing filter provides a useful bandwidth of up to 2700 Hz at 6000 Hz sampling, and so this is sufficient for most routine mine seismic monitoring purposes.

The power consumption of the GS seismic station is very low at 3 W, making the unit suitable for battery-powered monitoring applications. An integrated Uninterruptable Power Supply powers the GS for at least 6 hours in case of power failure, and the seismograms can be stored locally on a USB flash drive and internal non-volatile memory before the power is lost. In this way valuable seismograms of a large seismic event are preserved even if power and communications are disrupted after the event.

Figure 13: The GS seismic data acquisition unit from ISS International. With a frequency bandwidth of 0.3 - 48000 Hz and a dynamic range of 129 dB at 6000 Hz sampling rate, this seismic station meets the requirements of the typical seismic monitoring system. The unit is compact (140 mm $\times$ 200 mm $\times$ 65 mm) and has a power consumption of 3 W. Digital seismogram data is transmitted to the central site and can also be stored locally on a USB disk.

Most mines around the world do not require seismic-monitoring equipment that is certified to operate in explosive gas (methane) environments. The GS stations use 3 W of power, and since this much power is sufficient to make an electrical spark, heavy explosive-proof enclosures must be used for the GS in such environments.

Alternatively, the GSi unit can be used in such mines with explosive gases present. This unit is a full seismic station, sampling at 5000 Hz with a 24-bit digitiser and using less than 0.11 W of power. Since the power consumption is so low, this unit does not require any explosion-proof box and has been certified for use in Russian and South African mines.

Figure 14: The GSi seismic data acquisition unit from ISS International. This unit is a full seismic station that uses less than 0.11 W of power and has been certified for use in explosive gas environments. The unit is very compact (130 mm $\times$ 80 mm $\times$ 30 mm) and records digital seismograms from a tri-axial geophone at a sampling rate of 5000 Hz.

The ISS seismic system is usually permanently installed at locations underground, as close as practically possible to the working areas given the constraints of cabling for power and communications. To get seismic sensors even closer to the zone of rock which is being most influenced by mining, the GSx wireless seismic stations can be used. These units have an internal rechargeable battery, digital radio and 14 Hz geophone, and communicate with the closest GS seismic station using any other GSx units as relays. This Internet-style of self-configuring communications makes the units very easy to install, and the internal battery powers the device for over 3 weeks. The device can measure non-seismic sensors (for example convergence meters) or the uni-axial geophone. For the seismic data, the signal is sampled and analysed within the GSx unit, and the micro-seismic activity rate is transmitted back to the central site each minute.

Digital seismogram data at the central site computer is processed interactively with the JMTS software package to estimate the location, inelastic co-seismic deformation, P, and radiated seismic energy, E, for each seismic event. Figures 10 and 11 show screen-shots of this software. In addition, some secondary parameters are extracted for each event, such as the corner frequency, f_0, and inelastic attenuation parameter, Q.

Figure 15: The wireless GSx seismic data acquisition unit from ISS International. This unit monitors an internal 14 Hz uni-axial geophone and reports the micro-seismic activity rate to the closest GS each minute. The device is powered from a rechargeable internal battery and communicates via a spread-spectrum digital radio, using other GSx units as relays if necessary. The device has bright lights that can be turned on remotely to warn local users of unusual micro-seismic activity rates.

These seismological parameters for each event are then analysed, as discussed in Section 3. Once a group of seismic events have been processed and quantified, an analysis of seismicity is possible. This was described in Section 5 and is achieved using the custom-built 3-D visualisation and seismological analysis software - JDi.

7 Conclusions

This paper has presented the methodology of routine seismic monitoring for mines, as currently in use at over 150 mines in 30 countries. The most common objectives of rescue, prevention, seismic hazard rating and alerting, warning and back-analysis were explored. While monitoring requirements for the objective of rescue is not stringent as only the largest events need to be located, even very small events must be recorded and quantified for the objective of warning to be feasible. Thus the required seismic system must be specified with the overall monitoring objectives in mind.

In order to achieve any of these objectives, seismic events must be routinely located in relation to the 3-dimensional geometry of the mine workings and the source parameters must be quantified. The source size limits the accuracy of location, as the rupture can start anywhere on the eventual fault surface. Notwithstanding this, typical 3-D location errors of 3% of the average hypocentral distance should be possible with a modern seismic monitoring system and well-designed seismic array.

For each event, the radiated seismic energy E and co-seismic inelastic deformation P are independently estimated. From these measurements, it is possible to quantify the apparent stress drop, energy index and apparent volume of each seismic event. While the stress drop is commonly considered, it is however more useful to use energy index as a proxy for the dynamic stress levels within the rock surrounding a mine. The apparent volume provides a parameter with information about seismic deformation that scales more usefully than simple cumulative potency.

Moment tensor estimation is a powerful tool that is often used in seismological back analyses. The understanding of how large seismic events occur aids in the design of new mine levels in order to minimise the chances of recurring large seismic events. While this technique has proved to be the most difficult to implement routinely, new tools are constantly being developed to make this task simpler.

A group of seismic events can yield interesting conclusions when analysed jointly. Such is the basis for time history analysis of seismological parameters like energy index, cumulative apparent volume and seismic Schmidt number. Stability analyses of mining sections is routinely undertaken in mines around the world using such time history analysis.

Recently, high precision (10^{-6}) measurements of P-wave velocity variations have yielded promising precursory patterns prior to some large ($m_l = 1.0$ and $m_l = 3.0$) seismic events on the San Andreas fault (*Niu*

et al., 2008). This technique is being attempted in underground mines now (*Lynch*, 2010) and, if successful, would further increase the success rates of advance indications of potentially large instabilities in underground mines.

Modern digital seismic monitoring technology has evolved over the past 20 years. The large variation in both frequencies and amplitudes of seismic signals from mining induced seismicity means that a large dynamic range with low noise levels and high sampling rates are required. This is achieved by the use of distributed seismic stations underground. However in the mining environment, reliability of underground electronic equipment is of utmost importance. Given the extensive and often quite old telecommunications network underground, digital modems between distributed seismic stations and the surface central site must be robust and fault-tolerant, as well as flexible. These technical challenges drive the development of the latest seismic monitoring systems.

As developed as the methodology and technology of mine seismic monitoring is, the complexity of the subject requires a commitment from the mine in the form of a dedicated engineer or scientist who will operate the system. The full benefits of seismic monitoring in mines is attained when this person is prepared to say “I love my seismic system”(*Mikula*, 2005).

References

Aki, K. (1966), Generation and propagation of G waves from the Niigata earthquake of June 16, 1964. Part 2: Estimation of earthquake moment, released energy, and stress strain drop from the G-wave spectrum, *Bulletin Earthquake Research Institute Tokyo University*, *44*, 73–88.

Aki, K., and P. G. Richards (2002), *Quantitative Seismology*, 2nd ed., University Science Books, California.

Backus, G. E., and M. Mulcahy (1976), Moment tensor and other phenomenological descriptions of seismic sources. 1. Continuous displacements, *Geophys. J. R. Astron. Soc.*, *46*, 301–329.

Ben-Menahem, A., and S. J. Singh (1981), *Seismic Waves and Sources*, Springer-Verlag, New York.

Brune, J. N. (1968), Seismic moment, seismicity and rate of slip along major fault zones, *Journal of Geophysical Research*, *73*, 777–784.

Brune, J. N. (1971), Tectonic stress and the spectra of seismic shear waves from earthquakes: Correction, *Journal of Geophysical Research*, *76*, 5002.

Dubinski, J., and K. Stec (2001), Relationship between focal mechanism parameters of mine tremors and local strata tectonics, in *Proceedings of the 5th international symposium on rockbursts and seismicity in mines*, edited by G. van Aswegen, R. J. Durrheim, and W. D. Ortlepp, pp. 113–118, South African Institute of Mining and Metallurgy.

Gutenberg, B., and C. F. Richter (1956), Magnitude and energy of earthquakes, *Ann. Geofis.*, *9*, 1–15.

Hanks, T. C., and H. Kanamori (1979), A moment magnitude scale, *Journal of Geophysical Research*, *84*, 2348–2350.

Julian, B. R., A. D. Miller, and G. R. Foulger (1998), Non-double-couple earthquakes 1. Theory, *Reviews of Geophysics*, *36*(4), 525–549.

Kanamori, H. (1977), The energy release in great earthquakes, *Journal of Geophysical Research*, *82*(20), 2981–2987.

Kanamori, H., and D. L. Anderson (1975), Theoretical basis of some empirical relations in seismology, *Bulletin of the Seismological Society of America*, *65*(5), 1073–1095.

Keilis-Borok, V. I. (1959), On estimation of the displacement in an earthquake source and of source dimensions, *Annali di Geofisica*, *12*(2), 205–214.

King, G. C. P. (1978), Geological faults, fractures, creep and strain, *Philosophical Transactions of the Royal Society of London. Series A, Mathematical and Physical Sciences*, *288*(1350), 197–212.

Kostrov, B. V. (1974), Seismic moment and energy of earthquakes and seismic flow of rock., *Izv. Phys. Solid Earth*, *13*, 13–21.

Kostrov, B. V., and S. Das (1988), *Principles of Earthquake Source Mechanics*, Cambridge University Press.

Lynch, R., and D. Malovichko (2006), Seismology and slope stability in open pit mines, in *International Symposium on Stability of Rock Slopes*, International Symposium on Stability of Rock Slopes.

Lynch, R., and A. Mendecki (2004), Gap601a: Experimental and theoretical investigations of fundamental processes in mining induced fracturing and rock instability close to excavations - research project for safety in mines research advisory council, *Tech. rep.*, ISS International Limited.

Lynch, R., and A. J. Mendecki (2001), High-resolution seismic monitoring in mines, in *Proceedings of the 5th International Symposium on Rockbursts and Seismicity in Mines, Johannesburg, South Africa*, edited by G. van Aswegen, R. J. Durrheim, and W. D. Ortlepp, pp. 19–24, South African Institute of Mining and Metallurgy.

Lynch, R., R.A..and Wuite, B. Smith, and A. Cichowicz (2005), Microseismic monitoring of open pit slopes, in *Rockbursts and Seismicity in MInes 6, Perth*, edited by Y. Potvin and M. Hudyma, Australian Centre for Geomechanics.

Lynch, R. A. (2010), Keynote address: Passive and active microseismic monitoring in mines, in *Proceedings of the 5th Deep and High Stress Mining Seminar, Santiago, Chile*.

Malovichko, D. A., and R. A. Lynch (2006), Micro-seismic monitoring of open-pit slopes, *Mining Echo*, *2*(24), 21–30.

McGarr, A. (1991), Observations constraining near-source ground motion estimated from locally recorded seismograms, *Journal of Geophysical Research*, *96*(B10), 16,495–16,508.

Mendecki, A. J. (1993), Real time quantitative seismology in mines: Keynote address, in *Proceedings of the 3rd International Symposium on Rockbursts and Seismicity in Mines, Kingston, Ontario, Canada*, edited by R. P. Young, pp. 287–295, Balkema, Rotterdam.

Mendecki, A. J. (1997a), Quantitative seismology and rock mass stability, in *Seismic Monitoring in Mines*, edited by A. J. Mendecki, 1 ed., chap. 10, pp. 178–219, Chapman and Hall, London.

Mendecki, A. J. (Ed.) (1997b), *Seismic Monitoring in Mines*, 1 ed., 262 pp., Chapman & Hall.

Mendecki, A. J. (2001), Data-driven understanding of seismic rock mass response to mining: Keynote Address, in *Proceedings of the 5th International Symposium on Rockbursts and Seismicity in Mines, Johannesburg, South Africa*, edited by G. van Aswegen, R. J. Durrheim, and W. D. Ortlepp, pp. 1–9, South African Institute of Mining and Metallurgy.

Mendecki, A. J., G. van Aswegwn, and P. Mountfort (1999), A guide to routine seismic monitoring in mines, in *A Handbook on Rock Engineering Practice for Tabular Hard Rock Mines*, edited by A. J. Jager and J. A. Ryder, chap. 9, pp. 287–309, The Safety in Mines Research Advisory Committee, Johannesburg.

Mikula, P. A. (2005), The practice of seismic management in mines – how to love your seismic monitoring system, in *Rockbursts and seismicity in mines: Proceedings of the 6th International Symposium*, edited by Y. Potvin and M. Hudyma, Australian Centre for Geomechanics.

Mountfort, P., and A. J. Mendecki (1997), Seismic transducers, in *Seismic Monitoring in Mines*, edited by A. J. Mendecki, 1 ed., chap. 1, pp. 1–20, Chapman and Hall, London.

Niu, F., P. G. Silver, T. M. Daley, X. Cheng, and E. L. Majer (2008), Preseismic velocity changes observed from active source monitoring at the parkfield safod drill site, *Nature*, *454*.

Takei, Y., and M. Kumazawa (1994), Why have the single force and torque been excluded from seismic source models?, *Geophys. J. Int.*, *118*, 20–30.

Trifu, C. I., D. Angus, and V. Shumila (2000), A fast evaluation of the seismic moment tensor for induced seismicity, *Bulletin of the Seismological Society of America*, *90*, 1521–1527.

USGS (1996), http://quake.wr.usgs.gov/recenteqs/beachball.html, *Tech. rep.*

van Aswegen, G., and A. G. Butler (1993), Applications of quantitative seismology in South African gold mines, in *Proceedings of the 3rd International Symposium on Rockbursts and Seismicity in Mines, Kingston, Ontario, Canada*, edited by R. P. Young, pp. 261–266, Balkema, Rotterdam, iSBN 90 5410320 5.

Voinov, K. A., and V. G. Selivonik (1998), Estimation of stresses and mobility of structural blocks according to processing of mechanisms of seismic event sources, in *Mining Geophysics*, pp. 86–91, VNIMI.

Wyss, M., and J. N. Brune (1968), Seismic moment, stress and source dimensions for earthquakes in the California-Nevada region, *Journal of Geophysical Research*, *73*, 4681–4694.

Younga, S. L., and Y. V. Fedotova (2000), Study of source mechanisms of low energy seismic events in khibiny massif, in *Proceedings of the All-Russian Geodynamics and Technogenesis meeting*, pp. 171–174.